Topics in Catalysis
https://doi.org/10.1007/s11244-021-01473-6

ORIGINAL PAPER

The Role of Zeolite Framework in Zeolite Stability and Catalysis from Recent Atomic Simulation

Sicong Ma[1] · **Zhi-Pan Liu**[1]

Accepted: 8 July 2021

Abstract
Zeolite is a class of microporous crystalline materials widely used in heterogeneous catalysis. Over the past decades, theoretical simulations, particularly those based on first principles calculations, have advanced significantly the understandings on zeolite, from structure to adsorption kinetics and to catalytic reactivity. The machine learning (ML) methods developed in recent years further boost the ability of theory for unraveling the interplay between the synthetic conditions and the zeolite structure and functionality. This short review overviews the theoretical insights into the role of zeolite framework in zeolite stability and catalysis revealed from atomic simulation in recent years. We will mainly focus on two key aspects: (i) the theory on zeolite stability, including the templating effect of structure directing agents and the zeolite bonding pattern analysis; (ii) the confinement effect of zeolite pores that affects the catalytic conversion of molecules in zeolite. The future directions of theoretical simulation are also discussed.

Keywords Zeolite · Synthesis · Catalysis · Machine learning · Density functional theory

1 Introduction

Zeolite is an important class of inorganic crystalline materials built exclusively by the corner-sharing TO_4 tetrahedra (T denotes tetrahedrally coordinated Si, Al, or P, etc.). It has been widely used in many fields of chemistry, particularly important as the catalysts in the fields of petroleum chemistry and fine chemical industry. According to the simple packing rule of TO_4 tetrahedra, a rich variety of zeolite structures are likely, i.e. millions of hypothetical zeolite structures from recent predictions [1–3], but only 252 distinct zeolite structures (*IZC-SC* database) [4] have been successfully synthesized in the past century. Synthetic efforts have been more focused on zeolites with unconventional structural features, such as extra-large pores, low framework density, extremely complex framework topology and intrinsically chiral frameworks, etc.

In tradition, zeolite synthesis follows the hydrothermal method, where a large parameter space of synthetic conditions helps to control the complex crystallization kinetics and yield the metastable porous crystal. The hydrothermal crystallization from the alkaline solution mixture containing silicon, aluminum and alkali metals only leads to aluminosilicate zeolite with low Si:Al ratio (e.g. <5), where the strong alkali (OH^-) acts as the key mineralizer to dissolve Si and Al ions [5–7]. The replacement of inorganic alkalis by tetramethylammonium as the structure directing agents (SDAs) found by Barrer et al. [8] breaks the Si:Al ratio limitation to obtain even pure SiO_2 zeolites (e.g. ZSM-5) [9]. The pure SiO_2 zeolites can also be produced using the recently-reported solvent-free synthetic route [10, 11]. The aluminophosphate zeolite (AlPO) that enters into the zeolite family in 1980s [12] utilizes boehmite, phosphoric acid and organic amine as reagents. To date, the synthesis of novel zeolite is still largely governed by domain heuristics acquired through experience and is thus rather labor intensive during the testing of various synthetic conditions, such as the feed Si:Al:P ratios, pH values and SDAs, the crystallization temperature and time [13–16]. It would be desirable to speed up the discovery of new zeolites by predicting the synthetic conditions and route from theory.

✉ Zhi-Pan Liu
zpliu@fudan.edu.cn

[1] Shanghai Key Laboratory of Molecular Catalysis and Innovative Materials, Key Laboratory of Computational Physical Science, Department of Chemistry, Collaborative Innovation Center of Chemistry for Energy Material, Fudan University, Shanghai 200433, China

Published online: 13 July 2021

Zeolites possess a range of interesting properties, for example the good thermal/hydrothermal stability at high temperatures, the confinement of micropores, and the unique solid acidic/basic sites. They have been utilized not only for catalyzing directly the catalytic conversion but also as the microporous reactor to load the metal clusters. The 1962 witnessed the landmark achievement in zeolite catalysis, where the synthetic faujasites (zeolites X and Y) was first introduced in the fluid catalytic cracking (FCC) of heavy petroleum distillates that increase significantly the yield of gasoline [17]. To date, zeolite catalysts have conquered many important processes in petroleum refining and chemical conversion, including hydrocracking, light gasoline isomerization, methanol-to-hydrocarbons (MTH) and methanol-to-olefins (MTO) technologies, etc. [18–20]. These industrial applications, in turn, asked for the deep knowledge on zeolite structure and activity, where the state-of-the-art experimental and theoretical tools were applied to provide the atomic-level information through the years [21].

Theoretical simulations, particularly in the framework of density functional theory (DFT) calculations, reshape largely the material simulation and catalysis community in the past 30 years. It has become an essential complement to experiment for understanding catalyst structures and reaction activity [22, 23], and has been used to model and predict various properties of zeolites, from structure to reactivity. On the other hand, DFT simulations are generally frustrated in modeling large systems (> 100 atoms) at the long-time scale (> 10 ns), which leads to their limited predictive power for many key properties, particularly those relating to zeolite synthesis (e.g. nucleation, growth and dissolution). For molecules interaction with zeolite, the accuracy of DFT calculations also raised severe concerns for the poor description of van der Waals (vdw) interaction in DFT. To overcome the deficiencies of DFT calculations, new theoretical methods have been developed in recent years. As a representative, the machine learning (ML) techniques [24–26] has been adopted successfully in studying zeolite. The ML models have demonstrated their great values in finding the correlation between complex synthesis conditions and the zeolite type [27–29]. This circumvents the difficulty of atomic simulations in directly simulating the zeolite synthesis. The ML methods have also been utilized to predict mechanical properties [30] and explore the optimum SDAs [31].

An important breakthrough in atomic simulations is the advent of global ML potentials for describing the global potential energy surface (PES) of zeolite. The ML potential simulation can reach the accuracy of DFT calculations but with the speed of several orders of magnitude faster and thus can be utilized for long-time simulation of large systems. In 2018 our group developed the first global neural network (NN) potential simulation package, LASP software (Large-scale atomic simulation with neural network Potential, accessible from http://www.lasphub.com) [32], which integrates the PES data generation from DFT, the NN potential training and the atomic simulation in one platform. By using LASP, a large set of NN potentials, including the five-element Si–Al–P–O–H NN potential [33] for zeolite, are established via the automated global-to-global learning procedure, which can fast and accurately evaluate the PES and facilitate to address the thermodynamics and kinetics problems of complex materials.

Admittedly, the chemistry of zeolite is now an extensive topic with numerous literatures. This review will mainly focus on the role of zeolite framework in sustaining the zeolite high stability and facilitating catalysis as revealed from recent atomic simulation. We would like to refer the readers to many excellent reviews in the zeolite field, for example zeolite synthesis [34–36], catalytic reactions [17, 37, 38], simulation method advances [39, 40] and the discussions about key properties of zeolite (e.g. acidity and cation sites etc.) [41–47]. This review is organized as follows. Section 2 overviews the recent advances in understanding the formation of zeolite framework, including the templating effect of SDAs and the zeolite stability analysis. The interaction of zeolite framework with confined molecules, as encountered in catalysis, is discussed in Sect. 3, which includes three parts, i.e. the current status on the calculation accuracy, the free energy calculation at high temperatures, and the confinement effect of zeolite framework.

2 Theoretical Advances in Understanding Zeolite Stability

The zeolite formation is generally believed to consist of two stages: the aggregation of small silicate and aluminate to form alumino-silicate polymers, and the assembly of alumino-silicate polymers to create the zeolite skeleton that could be mediated by SDAs, as schematically shown in Fig. 1. The silicate/aluminate condensation and nucleation starts from the reaction between $Si(OH)_4$ and $Si(OH)_3O^-$ monomers, where the anion attacks the neutral species to form an intermediate structure containing a fivefold coordinated Si center. The reaction barrier and the reaction energy vary from 0.36 to 1.27 eV and − 0.49 to 0.81 eV, respectively, which is strongly affected by the solvent environments as calculated by previous DFT calculations [48–51]. Upon water removal, a negatively charged dimer is formed, followed by the continuous polymerization. The Al–Si dimer condenses either with the $Al(OH)_4Na$ monomers to form the Al–Si–Al trimer or with another Al–Si dimer to form the Al–Si–Al–Si tetramer [52]. After that, the alumino–silicate polymers are then wrapped outside SDAs for the further polymerization to zeolite skeleton.

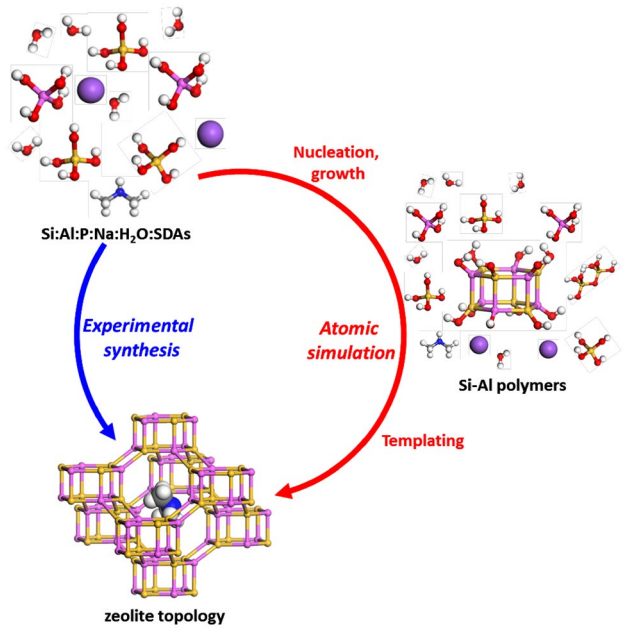

Fig. 1 Sketch Map of zeolite formation process

The atomic simulation at this stage becomes difficult due to the large system involved and the long time scale in order to form the zeolite 3D framework. Below in Sect. 2.1 we will first overview the current opinions for the role of SDAs, which are regarded as the core component to determine the type of zeolite skeleton. The other factors to affect the zeolite stability are discussed in Sect. 2.2.

2.1 Templating Effect of SDAs

The presence of SDAs is of central importance for the zeolite synthesis. In particular, the types of the high-silica and aluminophosphate zeolites are very sensitive to the choice of SDAs [14]. The trial-and-error with different SDAs is often one of the most efficient ways for synthesizing novel zeolite structures in experiment. To date, various types of SDAs have been developed, including both alkaline metal ions and organic SDAs (e.g. N-contained SDAs, P-containing SDAs, imidazolium derivatives, and metal complexes).

The previous DFT calculations have shown that the most effective SDAs observed in experiment generally has the highest binding energy with the target zeolite skeleton [47]. Both hydrogen bonding (H-bond) and ionic interactions affect the binding strength between SDAs and zeolite. Theoretical methods are therefore developed to screen out the optimal SDAs with the highest binding energy with zeolite skeleton. For example, Lewis et al. [53] developed the *Zebeddee* code to search for SDA numerically to best fit into the target zeolite skeleton that works as the template. The procedure starts by seeding an initial molecule to which functional groups from a fragment library are added selectively; a range of operations are then followed, including bond rotation and translation, to fulfill energy minimization. The optimal SDA is finally generated by comparing the overall stability between different candidates. Similar numerical approaches have also been developed, e.g. as implemented in ZEOMICS [54] and Zeo++[55] codes. While, Deem et al. [31] developed a ML approach to predict the binding energy of SDA. They pointed out that there are 469 SDAs with verified stabilization energies below − 17 kJ mol^{-1} Si^{-1}, comparable to or even better than widely used SDAs for zeolite Beta. It indicates that only calculating the binding energy between SDAs and zeolite framework does not necessarily lead to the optimal SDAs.

Due to the lack of the global PES information, these enumeration approaches, however, cannot guarantee the target zeolite with the optimal SDA being indeed the most stable structure, i.e. the global minimum, and thus may lead to the wrong prediction of the experimental product. By using NN based global PES exploration, Ma et al. [33] constructed a global AlPO PES including from two-dimensional layered structures to caged and three-dimensional densely-packed structures, as illustrated in Fig. 2a. They introduced an external rigid body to mimic the short-range repulsive interaction between SDAs and zeolite skeleton (Fig. 2b). From that, they demonstrated that the zeolites with the specific skeleton could be the thermodynamically stable products in the presence of suitable SDAs. The increase of rigid body size (r_s) rapidly decreases the framework density value (Fig. 2c). Too large or too small r_s fail to identify zeolite, leading to either the two-dimensional layered or the three-dimensional densely-packed structures. The zeolite only turns out to be the global minimum under the suitable r_s being applied, i.e. in between 3.5 and 5.5 Å. The four known zeolites, i.e. *ATV-, ATO-*, *ATS-* and *CHA*-type, do emerge as the global minimum at $r_s = 3.5$, 4, 4.5 and 5–5.5 Å, respectively. The choice of SDAs with the suitable size is indeed the key to condense TO_4 towards the desirable zeolite structure, instead of other stable phases.

With the advent of NN potential calculations, it is conceivable that the design of SDAs can be greatly benefited in the future, not only in evaluating the binding energy but also in quantifying the global minimum. The major obstacle is still the development of multi-element NN potentials to mimic zeolite synthesis, which need to include at least the five elements Si–Al–P–O–H of zeolite framework and the additional elements in SDAs such as C–N–P elements.

2.2 Thermodynamic Stability of Zeolite

Owing to the metastable nature of zeolite (as compared to densely-packed quartz SiO_2), it has taken a long effort to reveal the origin for the high thermal stability of zeolite

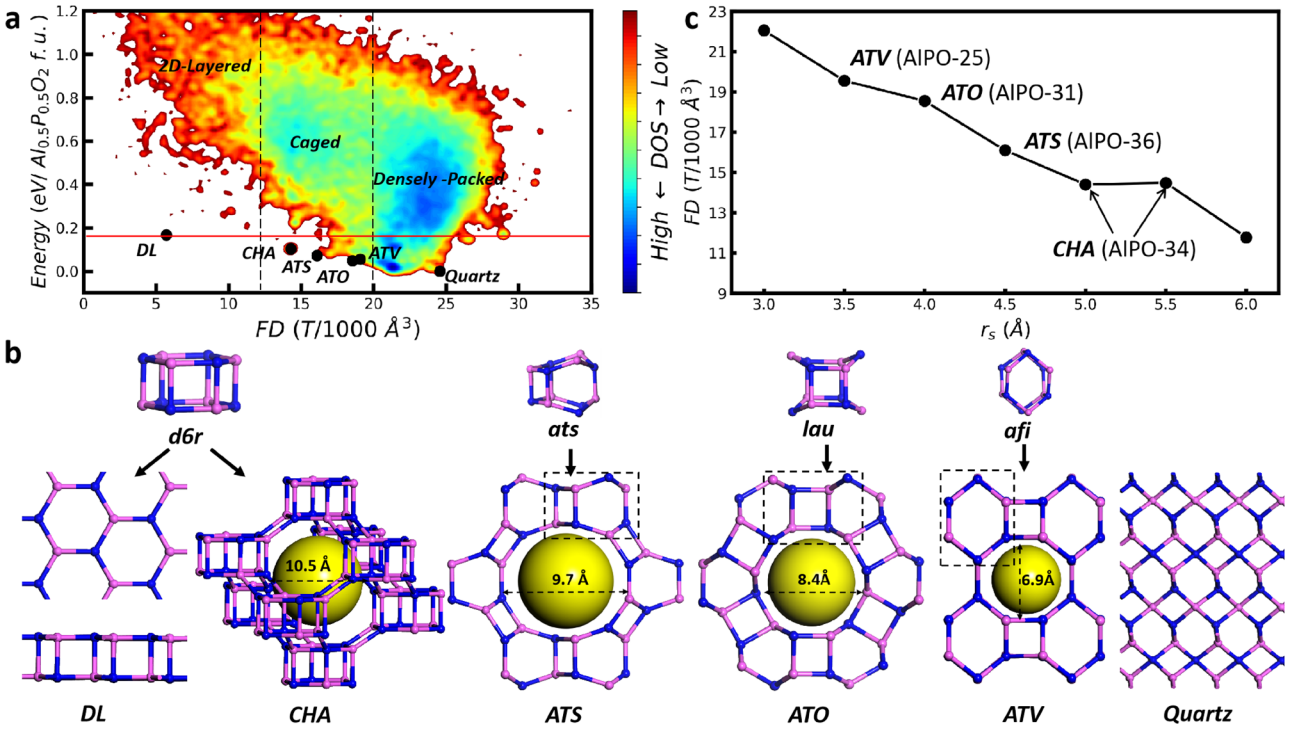

Fig. 2 Global PES exploration based on G-NN potential. **a** Global PES contour plot of $Al_6P_6O_{24}$ minima. The **x** axis is the framework density (FD), the **y** axis is the total energy of minima with respect to global minimum (quartz phase). **b** Key low energy crystalline structures. Yellow sphere indicates zeolite void. **c** The variation of the global minimum structures identified from global search in the presence of rigid body at different rigid body size *(r_s)* value. Reprinted with permission from Ref. [33]

framework. The fundamental understandings achieved have facilitated to answer important questions in zeolite design, for example, whether a particular hypothetical zeolite structure can be synthesized in reality. In history, scientists first analyzed and learned the underlying distinguishable features shared by all existing zeolites, and made attempts to extend these understandings to hypothetical zeolites.

The energy criterion is often utilized as the essential index in evaluating the relative stability. Bushuev et al. proposed two empirical criteria to assess thermodynamic feasibility: the upper energetic limit of ~ 0.17 eV per SiO_2 formula units (f.u.) and the ratio of energy and volume (ΔE/V) less than 0.5 kJ cm^{-3} (ΔE and V is the relative energy to quartz phase and zeolite volume, respectively) [56]. By exploring AlPO global PES, Ma et al. provided a physically-meaningful explanation of upper energy limit (Fig. 2a) [33]. If a caged structure is less stable than the two-dimensional layered structure, the presence of SDAs would explode the cage structure, resulting in the formation of two-dimensional layered structure. Therefore, the energy of two-dimensional layered structure determined the upper energy boundary. In their works, a 0.18 eV per $AlPO_4$ f.u. above quartz phase is identified as the upper energy boundary (red line in Fig. 2a), being consistent with the value suggested by Bushuev et al. [56]

Besides the energy criterion, the structural criterions are proposed to analyze the feasibility of zeolite. A linear relationship between the energy and the framework density value was discovered for conventional silicate zeolites [57–59]. However, with the emergence of many high-energy zeolites, especially unconventional zeolites containing T elements other than Al, Si, and P, the linear energy criterion is no longer reliable [56]. Many zeolites that are energetically not favored as silicates have been successfully realized as germanates [35]. Gramlich-Meier and Meier found that the T-O distances, O-T-O angles, T-O-T angles, and O-T-O-T-O twisting angles in feasible zeolite frameworks should vary within very narrow ranges [60]. Thorpe et al. [61] found that many existing zeolite frameworks showed a 'flexibility window' over a range of densities, but soon afterwards they found that several existing zeolites violates this rule.

In 2013, Yu et al. discovered that the local interatomic distances (LIDs) in all existing zeolite frameworks strictly obey a set of rules, which could be used to discriminate feasible zeolite structures from infeasible hypothetical structures [62]. Three types of LIDs were calculated, including D_{TO} (T-O distance), D_{OO} (O-T-O distance), and D_{TT} (T-O-T distance). They found that the average LIDs (designated $\langle D_{TO} \rangle$, $\langle D_{OO} \rangle$, and $\langle D_{TT} \rangle$, respectively) were linearly well

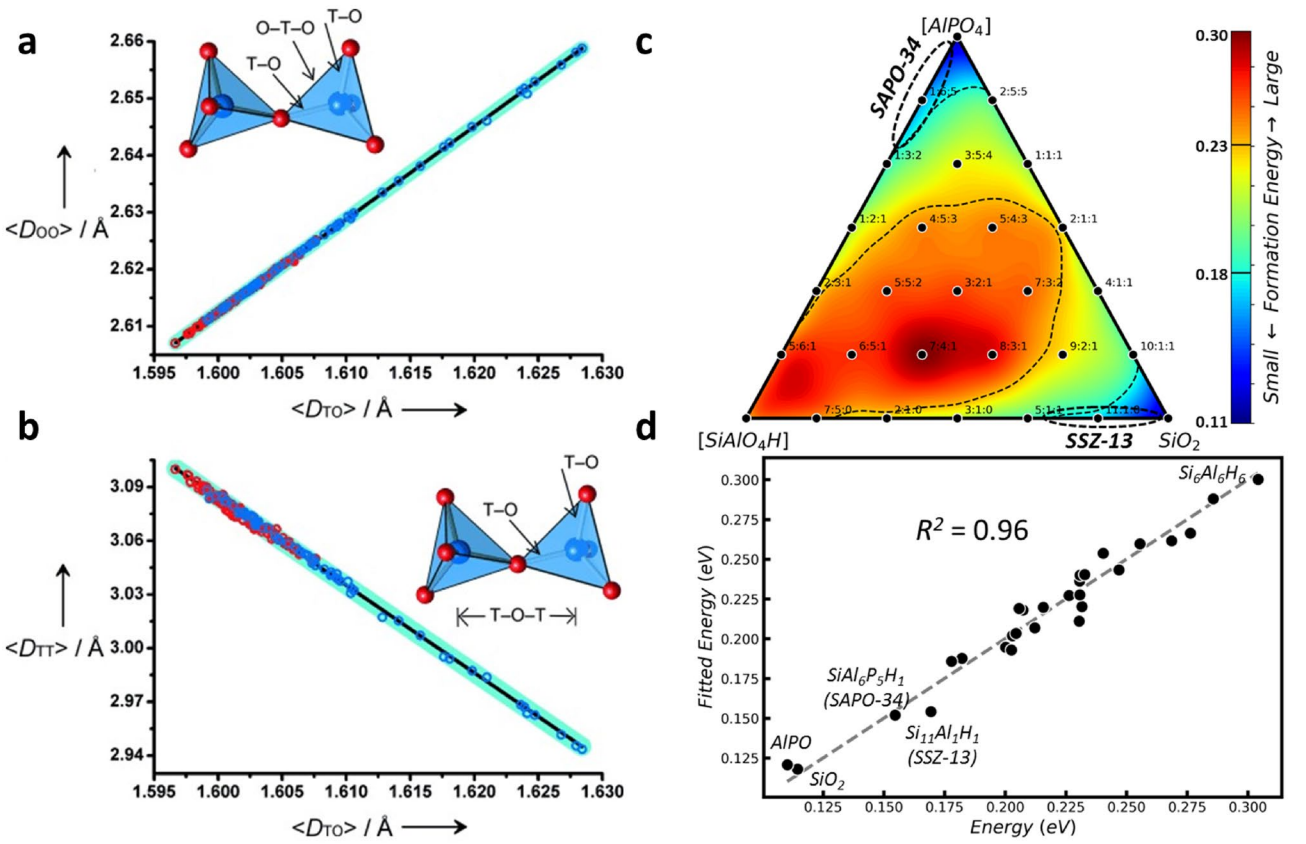

Fig. 3 **a**, **b** Linear relationships of **a** $\langle D_{OO} \rangle$ versus $\langle D_{TO} \rangle$ and **b** $\langle D_{TO} \rangle$ versus $\langle D_{TT} \rangle$ in existing zeolites. Reprinted with permission from Ref. [62]. **c** Gibbs formation free energy (G_f) contour plot in ternary phase diagram for varied $Si_xAl_yP_zO_2H_{y-z}$ composition. Si:Al:P ratio is indicated for each composition. **d** Correlation between G_f and the linear fitting of G_f (Eq. 1) for all data in (**c**). Reprinted with permission from Ref. [33]

correlated for all of the 200 existing zeolite frameworks (Fig. 3a and b). They then applied these LID criteria to evaluate the feasibility of 665 hypothetical zeolite frameworks derived from three different databases, and found that only 197 hypothetical zeolites are possibly synthesizable.

Beyond zeolite topology parameters, it has been observed that the zeolite stability also depends on the compositions and pH environments during the zeolite synthesis. Ma et al. constructed the thermodynamic ternary phase diagrams based on Gibbs formation free energy (G_f) with CHA-type SiO_2, AlPO and $SiAlO_4H$ as the vertexes, where H as the counter ions represent the neutral and acid pH environments (Fig. 3c) [33]. The minima appear nearby two vertexes, $Al_{0.5}P_{0.5}O_2$ and SiO_2, but the maximum appears at the left-bottom corner ($Si_{0.5}Al_{0.5}O_2H_{0.5}$). It proves the importance of Si:Al:P composition to the zeolite stability, causing the non-freely tunable Si:Al:P ratio in experiments. Moreover, a linear relationship is obtained by approximating G_f as the function of the proportions of TO_4 (monomer, P_T) and their linkages (T-O-T', $P_{TT'}$) based on their binding patterns, see Fig. 3d and Eq. 1. As G_f is positive in nature, it is no wonder that most terms, including monomers P_T terms, P_{SiP}, P_{AlAL} and P_{SiAl} terms have the positive energy contributions. But it is important to reveal that P_{SiSi} and P_{AlP} terms yield the negative contributions, suggesting they are the major driving forces to stabilize zeolite. The empirical rule in zeolite chemistry, namely, no Si–O–P and Al–O–Al patterns, is clearly manifested by their large positive prefactors, 0.35 and 0.16. In addition, the positive prefactor for P_{SiAl} term explains the difficulty to incorporate Si element in AlPO and the special Si:Al:P ratio of $n_{Si} < n_P$ in SAPO synthesized under neutral pH conditions.

$$G_f \approx (0.18 * P_{Si} + 0.20 * P_{Al} + 0.15 * P_P) + (0.35 * P_{SiP} + 0.16 * P_{AlAl} + 0.13 * P_{SiAl} - 0.06 * P_{SiSi} - 0.05 * P_{AlP}) \quad (1)$$

Moreover, the zeolite stability is also controlled by Al distributions, where the Al substitution energy is used as a thermodynamic energy criterion to evaluate the Al distributions. Muraoka et al. [63] found that the zeolite stability depends on the substituting contents of Al based on

Sanders−Leslie−Catlow interatomic potential calculation. The relation between the relative framework energies versus the Al contents varies in accordance with the topologies, suggesting that the relative stability of zeolites depends not only on the topologies, but also on the substituting contents of Al. The locations of Al in zeolites have a certain preference that zeolite with Al at a particular T site is energetically more stable than those with random distributions. The zeolite with Al atoms at particular lattice T sites is energetically more stable than that with random distributions. Similar phenomena have also been observed by others [64–66].

Compared to the zeolite stability analysis based on atomic simulation, the direct connection between synthesis conditions and target zeolite is also an insightful approach to reveal the origin of the zeolite stability. Jensen et al. [28] create natural language processing techniques and text markup parsing tools to automatically extract synthesis information and trends from 70,000 zeolite journal articles. They created a regression model for a zeolite's framework density from the synthesis conditions. This model has a cross-validated root mean squared error of 0.98 T/1000 $Å^3$, and many of the model decision boundaries correspond to known synthesis heuristics in germanium-containing zeolites. Muraoka et al. [29] trained ML XGBoost models to predict the zeolite skeleton based on parameters of the synthetic conditions from various literatures, as shown in Fig. 4. The experimental samples were first divided based on the Na/(Si + Al) ratio: zeolite structures obtained with high Na/(Si + Al) ratios included FAU, LTA, and SOD, and those such as MFI, MOR, and LTL obtained with lower Na/(Si + Al) ratios. The next boundary for the high Na/(Si + Al) groups was defined at the Si/(Si + Al) ratio of 0.5 (or Si/Al ratio = 1.) The three major phases observed in the branches with Si/Al > 1.0 were FAU, GIS, and ANA, which were separated clearly by the synthesis temperature. FAU was the most dominant phase at the lowest temperature, while ANA is dominated at the highest temperature. From that, they built a similarity network and uncovered the overlooked similarities between zeolites that were already manifested in the synthesis conditions.

Although the zeolite stability is controlled by not only thermodynamics but also kinetics, the latest atomic simulation evidences from global optimization emphasizes the importance of thermodynamics to the framework topologies and cation compositions, which are influenced by the synthetic conditions. Nevertheless, more theoretical efforts are desirable to probe the global energy landscape of different zeolites and identify the transformation pathway between zeolite. This additional kinetics information should further help to reveal the origin for the selectivity in forming different zeolite.

3 Atomic Simulations on the Zeolite–Molecule Interaction

Heterogeneous catalysis in zeolite involves the molecular diffusion, adsorption and reaction, which are influenced by many factors, including the zeolite framework type, acidic site, surrounding molecules and the temperature. The molecule–zeolite interactions are of the fundamental importance, which is however often very weak, being H-binding or vdw interaction. There has been a general concern on the accuracy of quantum chemistry (QM) methods in describing the zeolite catalysis [67–69]. In addition, most catalytic reactions on zeolite occur at high temperature (> 573 K), which will contribute a large entropy term to catalytic reactions, and thus free energy calculations are required to understand

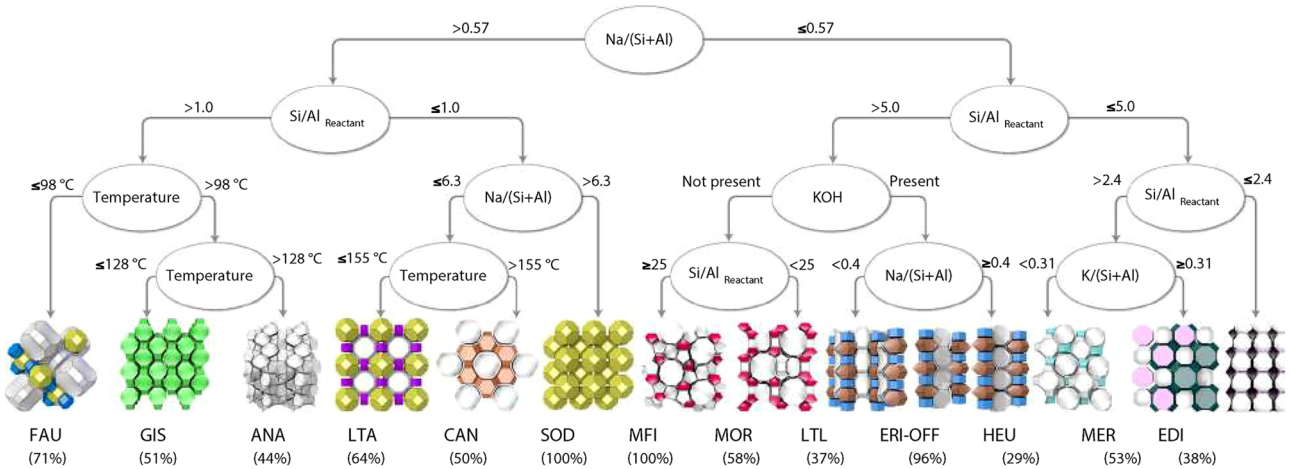

Fig. 4 Decision tree constructed from the trained XGBoost model. The percentages represent the fractions that the dominant phases appear in the deeper branches in the complete tree. Reprinted with permission from Ref. [29]

zeolite catalysis [70–72]. In this section, we first present the recent theoretical progress in improving the calculation accuracy and performing the free energy calculation, and with these knowledge on theoretical methods, we then review the current understandings on the confinement effect of zeolite.

3.1 Calculation Accuracy

It has been noticed that different theoretical methods can yield quite different adsorption energy of molecule in zeolite. For example, the adsorption energy of ethane in acid chabazite zeolite is vastly different from − 8 to − 56 kJ mol^{-1} according to different calculation methods [73]. Compared to the experimental data, the typical DFT calculations (e.g. Perdew–Burke–Ernzerhof functional, PBE) greatly underestimate the adsorption energy by 20–30 kJ mol^{-1}. This can be largely reduced with the post-DFT methods, although they generally are very demanding in computation. The random phase approximation (RPA) method underestimates the adsorption energy by only ~ 8 kJ mol^{-1}, whereas the and MP2 method leads to an overestimation by ~ 6 kJ mol^{-1} [73].

As a low-cost approach, the vdw correction is welcomed and widely used to improve the description of DFT for long-range interaction. Goltl et al. found that the DFT-vdw method can achieve the high calculation accuracy for ethane adsorption with the average errors of ~ 5 kJ mol^{-1} relative to experimental results [73]. While the DFT-vdw methods have now been popularly used in computing zeolite catalysis, there are rooms to improve the DFT-vdw accuracy, in particular, for evaluating the reaction barrier. Plessow and Studt compared the energy differences of reaction intermediates, including TS and minima between PBE-D3 and Møller–Plesset perturbation theory (MP2) methods. The reaction barriers with PBE-D3 were underestimated by ~ 30 kJ mol^{-1} relative to MP2 results and in some cases the deviations can be even more significant (~50 kJ mol^{-1}), e.g. the formation of $CH_3OCH_2OCH_3$ [68]. Interestingly, they also pointed out that although the PBE-D3 functional is prone to large errors in barrier, the predicted trends from one catalyst to another are good. They studied 65 reaction energies and 130 reaction barriers related to zeolite catalysis. The results showed that the total error for barriers between DFT and exact values is larger than 49 kJ mol^{-1}, but relative error between different catalyst is rather small (5 kJ mol^{-1}), as shown in Fig. 5. This validates the use of DFT-vdw calculations for fast screening and design of new catalytic materials [67].

More accurately, Sauer groups proposed a hybrid method combining the high-level QM method with the low-level DFT approach (MP2:(PBE + D2) + ΔCCSD(T)) to predict enthalpy barriers of periodic systems in the chemical accuracy (± 4 kJ mol^{-1}) [74–77]. Owing to the expensive

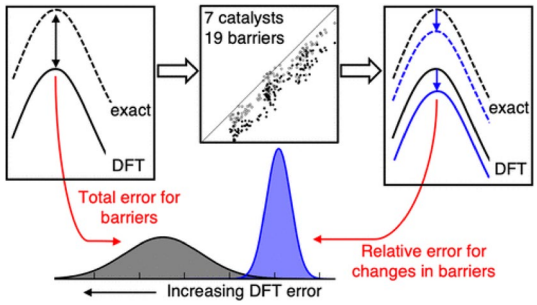

Fig. 5 The sketch map of energy differences between DFT and exact results. Reprinted with permission from Ref. [67]

calculation cost, these high precision methods are seldom utilized to treat complex catalytic reactions, which either requires to locate many reaction transition state (TS) or needs to invoke the high-temperature molecular dynamics (MD).

In recent years ML-based atomic simulation emerges as a promising tool, which can be trained to possess a high accuracy and in the meantime to achieve the high speed in evaluating energy [32, 78, 79]. The "high accuracy" of ML potential relies largely on the calculation accuracy of dataset calculated by various QM methods. Ma et al. constructed the SiAlPOH NN potential to explore the zeolite formation process with the calculation accuracy to PBE functional level [33]. The same framework should be applicable to construct more expensive post-DFT dataset. Recently, Bučko et al. [80, 81] presented an *ab-initio* approach that effectively couples perturbation theory and ML to make *ab-initio* free energy calculations more affordable. They implemented ML-based MD simulation to study the carbonylation reaction of methoxy groups in zeolite mordenite and the calculation accuracy reaches to the level of the hybrid HSE06 functional. From these latest works, the ML potential shows the promise to decrease dramatically the calculation cost and is well suited for complex catalysis problems.

3.2 Free Energy Calculations at High Temperature

A convinient way for computing the free energy is to evaluate the vibrational spectrum of the adsorbed molecules within the harmonic approximation. The approach, however, neglects the anharmonic vibrational contribution and also does not take into account the configuration entropy contribution. Wang et al. [82] investigated two different hydrocarbon pool mechanisms, i.e. aromatic-based and olefin-based cycles in H-SAPO-34 and H-SSZ-13, by using BEEF-vdw calculations. The Gibbs free energies were then calculated by correcting the DFT total energy with zero-point energy (ZPE) and entropy terms using the frequency calculation. They found the increase of the temperature from

0 to 673 K leads the increase of the apparent energy barrier of 20–50 kJ mol^{-1}.

The anharmonicity contribution to entropy can, however, be quite important, e.g. up to 15 kJ mol^{-1} [83–85]. Piccini et al. [86] calculated the reaction of methanol with ethene, propene, and trans-2-butene catalyzed by an acidic zeolite (H-MFI). The calculated enthalpy barriers at 623 K is slightly higher than the experiment results with the average errors of ~ 8 kJ mol^{-1} based on the hybrid QM:DFT methods. After introducing the anharmonic contributions, the average errors can be further reduced to 4 kJ mol^{-1}, which is now within the limit of chemical accuracy.

In order to take into account the configurational entropy, the long time MD simulation is required to collect the likely configurations at the target temperature. The enhaced MD is often utilized to increase the sampling at the high-energy states, such as the transition states. Bailleul et al. [87] investigated the methylation reaction of ethene with methanol over the Brønsted acidic ZSM-5 catalyst by using DFT-based MD simulation with the enhanced sampling methods at 673 K. The reaction kinetics obtained via various enhanced MD techniques agrees well with the intrinsic reaction rate constant in experiment. Bučko et al. combined the MD simulation with transition path sampling and free-energy integrations to obtain the free energy profiles of zeolite-related catalysis [88–90]. They found that the adsorption energy is considerably reduced at elevated temperature due to the weak specific interaction of the saturated molecule with Brønsted acid sites and that only a fraction of molecules within the zeolite can be sufficiently close to the acid site to allow the formation of the protonation precursor.

The QM-based MD calculations are computationally demanding, which requires to collect millions of PES points in MD trajectory. This is because different configurations are seperated with barriers and only long time MD simulation can help to obtain the converged results. The ML potential atomic simulation is the promising direction to speed up the free energy calculations [80].

3.3 The Confinement Effect of Zeolite

With the above knowledge on the theoretical progress, we now turn to the confinement effect of zeolite, which has been proposed to be one of the key merits of zeolite catalysis since 1960s [47, 91]. Recent years have seen the atomic simulation to verify the confinement effect from two aspects: the size matching between molecule and zeolite pore, and the local molecular accumulation in zeolite channels.

It was long suspected that the size matching between catalytic reactions and zeolite skeleton is the key to the success of zeolite catalysis, as explained in MTO with SAPO-34 zeolite, catalytic cracking with Y-type zeolite [17, 82]. The effect is however intricate and difficult to understood from simple morphology parameters, such as the pore size. Ghysels et al. investigated the diffusion of ethene through a series of 8-ring zeolites based on force field MD simulations [92]. The diffusion behaviors are quire different in different zeolite. For example, the diffusion coefficient in AlPO-18 is 10.2×10^{-10} m^2/s, much larger than that in SAPO-18 zeolite (1.9×10^{-10} m^2/s). The ring-dependent diffusion behavior cannot be described solely in terms of the composition and topology of the rings. Similar results have also been reported by others that small differences in ring size could lead to the big difference in molecular diffusion [93–95].

In addition to the molecule–zeolite interaction, the cage structure of zeolite can act as the trapping region to contain multiple molecules in one cage. This can significantly decrease the distance between molecules and the interactions between molecules could greatly affect the catalytic performance. For the molecular diffusion, Cnudde et al. [96] determined how molecular factors influence the diffusion of light olefins through the 8-ring windows of H-SAPO-34 based on MD simulation. They proved that the diffusion through the 8-ring is in general a hindered process, and thus the loading of multiple propene molecules in the cage can substantially facilitate the diffusion process. As shown in Fig. 6, in the case of two propene molecules in cage B the forward diffusion barrier is hardly affected (less than 4 kJ mol^{-1}). However, the backward diffusion barrier, i.e., from a cage with three propene molecules to an empty cage, substantially decreases due to the lower stability and reduced configurational freedom in cages with a higher propene loading. The diffusion barrier is lowered by nearly 20 kJ mol^{-1} in comparison to the reference case in the absence of additional propene molecules. For the highest loading, two additional propene molecules in both cage A and cage B, the diffusion barrier is also significantly lower (ca. 15 kJ mol^{-1}). This effect is also applied to bond making/breaking reactions. Nastase et al. [97] provided the mechanistic insight into the framework methylation within H-ZSM-5 at

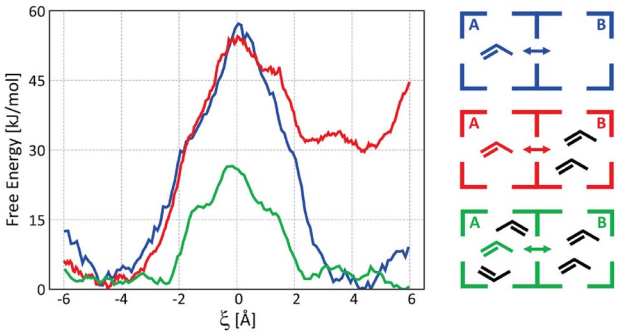

Fig. 6 Free energy profiles for propene diffusion through eight-membered ring of H-SAPO-34 at 600 K with different propene loadings in the cages from ab-initio MD simulation. Reprinted with permission from Ref. [96]

the high methanol loadings by varying the acid site densities. The MD simulation shows the formation of stable methanol clusters in the zeolite pores that can significantly decrease the methylation free-energy barriers from 142 kJ mol^{-1} with 3 MeOH to 112 kJ mol^{-1} with 5 MeOH.

Although the recent findings provide useful atomic level pictures for the confinement effect of zeolite, the quantitative rules to correlate the type of zeolite framework with catalytic reactions are still not established. It would be desirable to explore the confinement effect for different molecules in different zeolites via high-throughput atomic simulations. The future of theory should aim to predict the catalysis with a given reactants and to design the optimal zeolite framework for the reaction.

4 Perspective

Zeolite demonstrates its unique advantages in more and more modern catalytic applications. We here highlight recent theoretical advances of zeolite stability and catalysis based on first-principle and machine learning technologies. We have presented the current understandings of zeolite structure from thermodynamics to kinetics, and also discussed the major challenges in the atomic simulation. The recent ML applications in zeolite were also briefly overviewed, which covers both the atomic simulation based on the ML potential and the experiment-based ML to identify the best synthetic conditions for particular zeolite framework. These ML methods hold promise to solve the great complexity in zeolite structure and catalysis.

The next move of theoretical simulations on zeolite is clear, which should be along the line to further improve the accuracy of PES description and the sampling efficiency of PES. Because of the importance of weak intermolecular interaction in zeolite catalysis, it is highly desirable to reduce the cost of high-level post-DFT methods, in particular, in treating periodic systems as zeolite crystal. The free energy computation as required to properly address the high temperature and confinement catalysis needs to be equipped as a routine tool in the future, where the ML-based atomic simulations could be the key player.

The direct modeling of zeolite synthesis is perhaps the most challenging task to theoreticians, which is a long-term goal common to all subjects of chemical synthesis of materials. Ultimately, the explicit solvent, the ionic additives, the SDA molecules and the precursor reagents should be treated in one theoretical framework to account for the realistic (hydrothermal) synthetic environment, which then leads to resolve the kinetics origin for the diversity of zeolite framework. Fortunately, the advent of ML based on experimental data has brought attention to some key experimental conditions, which facilitates the simplification of the simulation model by focusing on the important synthetic parameters.

Acknowledgements This work was supported by the National Key Research and Development Program of China (Grant No. 2018YFA0208600), National Science Foundation of China (Grant Nos. 22033003, 21533001 and 91745201) and China Postdoctoral Science Foundation (Grant No. 2019M661340).

Declarations

Conflict of interest The authors declare no competing interests.

References

1. Treacy M, Rivin I, Balkovsky E, Randall K, Foster M (2004) Microporous Mesoporous Mater 74:121–132
2. Woodley SM, Catlow R (2008) Nat Mater 7:937–946
3. Pophale R, Cheeseman PA, Deem MW (2011) Phys Chem Chem Phys 13:12407–12412
4. IZC-SC database. http://www.iza-structure.org/databases/.
5. Ruren Xu, Pang W, Jihong Yu, Huo Q, Chen J (2007) Chemistry of zeolites and related porous materials: synthesis and structure. Wiley, New York, p 17
6. Yu J, Xu R (2010) Acc Chem Res 43:1195–1204
7. Cundy CS, Cox PA (2005) Microporous Mesoporous Mater 82:1–78
8. Barrer R, Denny P (1961) J Chem Soc 971–982
9. Argauer RJ, Landolt GR (1972) Crystalline zeolite ZSM-5 and method of preparing the same. US Patents 3,702,886
10. Jin Y, Sun Q, Qi G, Yang C, Xu J, Chen F, Meng X, Deng F, Xiao F-S (2013) Angew Chem Int Ed 52:9172–9175
11. Ren LM, Wu QM, Yang CG, Zhu LF, Li CJ, Zhang PL, Zhang HY, Meng XJ, Xiao FS (2012) J Am Chem Soc 134:15173–15176
12. Wilson ST, Lok BM, Messina CA, Cannan TR, Flanigen EM (1982) J Am Chem Soc 104:1146–1147
13. Burkett SL, Davis ME (1995) Chem Mater 7:920–928
14. Li J, Corma A, Yu J (2015) Chem Soc Rev 44:7112–7127
15. Dusselier M, Davis ME (2018) Chem Rev 118:5265–5329
16. Gallego EM, Portilla MT, Paris C, León-Escamilla A, Boronat M, Moliner M, Corma A (2017) Science 355:1051–1054
17. Vogt ETC, Weckhuysen BM (2015) Chem Soc Rev 44:7342–7370
18. Scherzer J, Gruia AJ (1996) Hydrocracking science and technology. CRC Press, Boca Raton
19. Ertl G, Knözinger H, Weitkamp J (1997) Handbook of heterogeneous catalysis, vol 2. Princeton, Citeseer
20. Chen N-Y (1996) Shape selective catalysis in industrial applications, vol 65. CRC Press, Boca Raton
21. Liu LC, Lopez-Haro M, Lopes CW, Li CG, Concepcion P, Simonelli L, Calvino JJ, Corma A (2019) Nat Mater 18:866–873
22. Liu ZP, Hu P, Alavi A (2002) J Am Chem Soc 124:14770–14779
23. Liu ZP, Hu P (2003) J Am Chem Soc 125:1958–1967
24. Ma S, Shang C, Liu Z-P (2019) J Chem Phys 151:050901
25. Ma S, Liu Z-P (2020) ACS Catal 10:13213–13226
26. Kang PL, Shang C, Liu ZP (2020) Acc Chem Res 53:2119–2129
27. Corma A, Diaz-Cabanas MJ, Moliner M, Martinez C (2006) J Catal 241:312–318
28. Jensen Z, Kim E, Kwon S, Gani TZH, Roman-Leshkov Y, Moliner M, Corma A, Olivetti E (2019) ACS Cent Sci 5:892–899

29. Muraoka K, Sada Y, Miyazaki D, Chaikittisilp W, Okubo T (2019) Nat Commun 10:4459
30. Kim N, Min K (2021) J Phys Chem Lett 12:2334–2339
31. Daeyaert F, Ye FD, Deem MW (2019) Proc Natl Acad Sci USA 116:3413–3418
32. Huang SD, Shang C, Kang PL, Zhang XJ, Liu ZP (2019) WIREs Comput Mol Sci 9:e1415
33. Ma SC, Shang C, Wang CM, Liu ZP (2020) Chem Sci 11:10113–10118
34. Moliner M, Rey F, Corma A (2013) Angew Chem Int Ed 52:13880–13889
35. Li Y, Yu J (2014) Chem Rev 114:7268–7316
36. Wang C, Xu J, Deng F (2020) ChemCatChem 12:965–980
37. Weckhuysen BM, Yu J (2015) Chem Soc Rev 44:7022–7024
38. Van Speybroeck V, De Wispelaere K, Van der Mynsbrugge J, Vandichel M, Hemelsoet K, Waroquier M (2014) Chem Soc Rev 43:7326–7357
39. Grajciar L, Heard CJ, Bondarenko AA, Polynski MV, Meeprasert J, Pidko EA, Nachtigall P (2018) Chem Soc Rev 47:8307–8348
40. Broclawik E, Kozyra P, Mitoraj M, Radon M, Rejmak P (2021) Molecules 26:1511
41. Gubbins KE, Liu YC, Moore JD, Palmer JC (2011) Phys Chem Chem Phys 13:58–85
42. Boronat M, Corma A (2014) Catal Lett 145:162–172
43. Mansoor E, Van der Mynsbrugge J, Head-Gordon M, Bell AT (2018) Catal Today 312:51–65
44. Li G, Pidko EA (2018) ChemCatChem 11:134–156
45. Wang S, He Y, Jiao W, Wang J, Fan W (2019) Curr Opin Chem Eng 23:146–154
46. Chizallet C (2020) ACS Catal 10:5579–5601
47. Van Speybroeck V, Hemelsoet K, Joos L, Waroquier M, Bell RG, Catlow CRA (2015) Chem Soc Rev 44:7044–7111
48. McIntosh GJ (2013) Phys Chem Chem Phys 15:17496–17509
49. Henschel H, Schneider AM, Prosenc MH (2010) Chem Mater 22:5105–5111
50. Trinh TT, Jansen APJ, van Santen RA, Meijer EJ (2009) Phys Chem Chem Phys 11:5092–5099
51. Trinh TT, Jansen APJ, van Santen RA, VandeVondele J, Meijer EJ (2009) ChemPhysChem 10:1775–1782
52. Yang CS, Mora-Fonz JM, Catlow CRA (2012) J Phys Chem C 116:22121–22128
53. Lewis DW, Willock DJ, Catlow CRA, Thomas JM, Hutchings GJ (1996) Nature 382:604–606
54. First EL, Gounaris CE, Wei J, Floudas CA (2011) Phys Chem Chem Phys 13:17339–17358
55. Willems TF, Rycroft C, Kazi M, Meza JC, Haranczyk M (2012) Microporous Mesoporous Mater 149:134–141
56. Bushuev YG, Sastre G (2010) J Phys Chem C 114:19157–19168
57. Akporiaye DE, Price GD (1989) Zeolites 9:321–328
58. Henson NJ, Cheetham AK, Gale JD (1994) Chem Mater 6:1647–1650
59. Brunner GO, Meier WM (1989) Nature 337:146–147
60. Gramlichmeier R, Meier WM (1982) J Solid State Chem 44:41–49
61. Sartbaeva A, Wells SA, Treacy MMJ, Thorpe MF (2006) Nat Mater 5:962–965
62. Li Y, Yu J, Xu R (2013) Angew Chem Int Ed 52:1673–1677
63. Muraoka K, Chaikittisilp W, Okubo T (2016) J Am Chem Soc 138:6184–6193
64. Vjunov A, Fulton JL, Huthwelker T, Pin S, Mei DH, Schenter GK, Govind N, Camaioni DM, Hu JZ, Lercher JA (2014) J Am Chem Soc 136:8296–8306
65. Wang S, Wang P, Qin Z, Chen Y, Dong M, Li J, Zhang K, Liu P, Wang J, Fan W (2018) ACS Catal 8:5485–5505
66. Li C, Vidal-Moya A, Miguel PJ, Dedecek J, Boronat M, Corma A (2018) ACS Catal 8:7688–7697
67. Plessow PN, Studt F (2020) J Phys Chem Lett 11:4305–4310
68. Plessow PN, Studt F (2017) ACS Catal 7:7987–7994
69. Gaggioli CA, Stoneburner SJ, Cramer CJ, Gagliardi L (2019) ACS Catal 9:8481–8502
70. Gounder R, Iglesia E (2012) Acc Chem Res 45:229–238
71. Van der Mynsbrugge J, De Ridder J, Hemelsoet K, Waroquier M, Van Speybroeck V (2013) Chem Eur J 19:11568–11576
72. Chen YY, Zhao XH, Qin ZF, Wang S, Wei ZH, Li JF, Dong M, Wang JG, Fan WB (2020) J Phys Chem C 124:13789–13798
73. Goltl F, Gruneis A, Bucko T, Hafner J (2012) J Chem Phys 137:114111
74. Berger F, Rybicki M, Sauer J (2021) J Catal 395:117–128
75. Rybicki M, Sauer J (2018) J Am Chem Soc 140:18151–18161
76. Tuma C, Sauer J (2015) J Chem Phys 143:102810
77. Sauer J (2019) Acc Chem Res 52:3502–3510
78. Behler J, Parrinello M (2007) Phys Rev Lett 98:146401
79. Bartók AP, Payne MC, Kondor R, Csányi G (2010) Phys Rev Lett 104:136403
80. Bucko T, Gesvandtnerova M, Rocca D (2020) J Chem Theory Comput 16:6049–6060
81. Gešvandtnerová M, Rocca D, Bučko T (2021) J Catal 396:166–178
82. Wang C-M, Wang Y-D, Du Y-J, Yang G, Xie Z-K (2015) Catal Sci Technol 5:4354–4364
83. Piccini G, Alessio M, Sauer J, Zhi Y, Liu Y, Kolvenbach R, Jentys A, Lercher JA (2015) J Phys Chem C 119:6128–6137
84. Piccini G, Sauer J (2014) J Chem Theory Comput 10:2479–2487
85. Alexopoulos K, Lee M-S, Liu Y, Zhi Y, Liu Y, Reyniers M-F, Marin GB, Glezakou V-A, Rousseau R, Lercher JA (2016) J Phys Chem C 120:7172–7182
86. Piccini G, Alessio M, Sauer J (2016) Angew Chem Int Ed 55:5235–5237
87. Bailleul S, Dedecker K, Cnudde P, Vanduyfhuys L, Waroquier M, Van Speybroeck V (2020) J Catal 388:38–51
88. Bučko T, Benco L, Hafner J, Ángyán JG (2011) J Catal 279:220–228
89. Bucko T, Benco L, Dubay O, Dellago C, Hafner J (2009) J Chem Phys 131:214508
90. Rey J, Gomez A, Raybaud P, Chizallet C, Bucko T (2019) J Catal 373:361–373
91. Moliner M, Roman-Leshkov Y, Corma A (2019) Acc Chem Res 52:2971–2980
92. Ghysels A, Moors SLC, Hemelsoet K, De Wispelaere K, Waroquier M, Sastre G, Van Speybroeck V (2015) J Phys Chem C 119:23721–23734
93. Chen D, Moljord K, Holmen A (2012) Microporous Mesoporous Mater 164:239–250
94. Dai WL, Scheibe M, Li LD, Guan NJ, Hunger M (2012) J Phys Chem C 116:2469–2476
95. Hedin N, DeMartin GJ, Roth WJ, Strohmaier KG, Reyes SC (2008) Microporous Mesoporous Mater 109:327–334
96. Cnudde P, Demuynck R, Vandenbrande S, Waroquier M, Sastre G, Van Speybroeck V (2020) J Am Chem Soc 142:6007–6017
97. Nastase SAF, Cnudde P, Vanduyfhuys L, De Wispelaere K, Van Speybroeck V, Catlow CRA, Logsdail AJ (2020) ACS Catal 10:8904–8915